

All-Optical Modulation Format Conversions from PAM4 to QPSK and 16QAM Using Silicon-Rich Nitride Waveguides

Yuto FUJIHARA[†], *Student Member*, Asahi SUEYOSHI[†], Alisson RODRIGUES DE PAULA^{††}, *Nonmembers*, Akihiro MARUTA[†], *Senior Member*, and Ken MISHINA^{†a)}, *Member*

SUMMARY Quadrature phase-shift keying (QPSK) and 16-quadrature amplitude modulation (16QAM) formats are deployed in inter-data center networks where high transmission capacity and spectral efficiency are required. However, in intra-data center networks, a four-level pulse amplitude modulation (PAM4) format is deployed to satisfy the requirements for a simple and low-cost transceiver configuration. For the seamless and effective connection of such heterogeneous networks without an optical–electrical–optical conversion, an all-optical modulation format conversion technique is required. In this paper, we propose all-optical PAM4 to QPSK and 16QAM modulation format conversions using silicon-rich nitride waveguides. The successful conversions from 50-Gbps-class PAM4 signals to 50-Gbps-class QPSK and 100-Gbps-class 16QAM signals are demonstrated via numerical simulations.

key words: optical signal processing, optical modulation, silicon photonics, silicon nitride

1. Introduction

The transmission capacity of metro data center (DC) interconnections that connect distributed DCs in a zone has increased rapidly. To satisfy the demand for high-capacity transmission, quadrature amplitude modulation (QAM) formats, such as quadrature phase-shift keying (QPSK) and 16QAM, are applied to metro DC interconnects [1], [2]. In contrast, the four-level pulse amplitude modulation (PAM4) format, which is a multilevel modulation format based on a cost-effective intensity modulation/direct detection transceiver, is implemented in short-reach networks such as intra-data-center networks [3]. Hence, modulation format conversions between PAM4 and QPSK or 16QAM signals are required to connect DCs in a zone, as illustrated in Fig. 1.

All-optical modulation format conversion is a promising technology for realizing low-latency and efficient network connections using different modulation formats [4], [5]. On-off keying (OOK) to PSK format conversions using semiconductor optical amplifiers (SOAs) and highly nonlinear fibers (HNLFs) were first proposed [6], [7]. Subsequently, modulation format conversions for multilevel signals, such as OOK to 16QAM [8], QPSK to PAM4 [9], and 16QAM

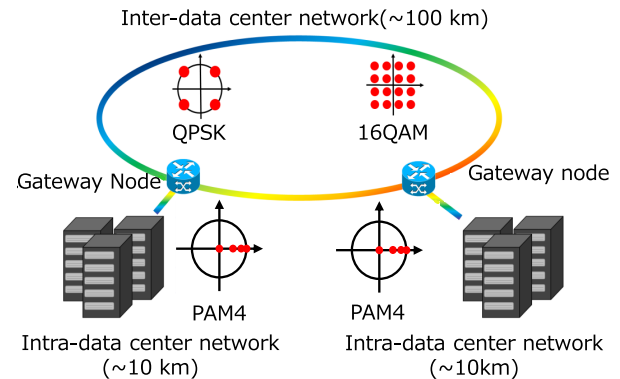


Fig. 1 Network connecting data centers.

to PAM4 conversions [10], have been reported. To connect intra-DC to inter-DC networks, all-optical PAM4 to QPSK and 16QAM format conversions using highly nonlinear fiber (HNLF) have been demonstrated [11], [12]. However, HNLF is limited in minimization because it is not applicable to photonic integrated circuits (PICs). For future photonic networks employing space division multiplexing with multicore fibers, HNLF-based converters encounter this problem on the footprint because an optical node needs to integrate a number of converters for a number of wavelength and space channels.

Recently, several nonlinear devices that can be integrated in PICs have been developed for optical signal processing. To realize power-efficient optical signal processing, nonlinear optical effects should be efficiently extracted. Although III-V compound semiconductors [6] and periodically poled lithium niobate [13] exhibit a highly efficient nonlinearity, the cost challenge remains owing to the complexity of the fabrication process. On the other hand, silicon (Si) photonics [14] based on a complementary metal oxide semiconductor (CMOS) platform has been attracting attention because this technology can help fabricate cost-effective PICs comprising Si and silicon nitride (SiN) waveguides on large-size Si-on-insulator (SOI) wafer. Although Si waveguides have a high nonlinear coefficient, the conversion efficiency is limited by two-photon absorption (TPA) in the communication wavelength band. SiN waveguides can avoid the TPA effect; however, their nonlinear coefficient is low, which requires special structures such as resonant structures and spiral-shaped waveguides.

To address this challenge, silicon-rich nitride (SRN)

Manuscript received January 5, 2023.

Manuscript revised April 6, 2023.

Manuscript publicized May 11, 2023.

[†]The authors are with the Graduate School of Engineering, Osaka University, Suita-shi, 565-0871 Japan.

^{††}The author is with the CORIA Laboratory, the French National Centre for Scientific Research (CSRS), the University of Rouen Normandie, Saint Etienne du Rouvray, 76801, France.

a) E-mail: mishina@comm.eng.osaka-u.ac.jp

DOI: 10.1587/transcom.2022OBP0003

waveguides with a high silicon ratio have been reported [15]–[17]. SRN exhibits superior performance as it enables a more flexible device engineering and higher Kerr nonlinearities than conventional stoichiometric silicon nitrides. Moreover, its bandgap is wider than that of Si, which can suppress the TPA effect. Although the material and manufacturing process of SRN waveguides have been actively studied, studies regarding their application in optical communication systems are insufficient. For example, the wavelength conversion of OOK signals [18] and the simultaneous wavelength conversion of wavelength division-multiplexing QPSK signals [19] have been reported. However, optical modulation format conversions using SRN waveguides are yet to be conducted.

In this paper, we propose all-optical modulation format conversions from PAM4 to QPSK and 16QAM, which can be realized cost-effectively on PICs based on cross-phase modulation (XPM) in SRN waveguides. The design of the SRN waveguide for the modulation format converter and the feasibility of the proposed conversion method are verified via numerical simulations. As an extension of the extant research in [20], we comprehensively describe the SRN waveguide design method for the proposed modulation format conversion together with theoretical and numerical investigations of the basic characteristics. Subsequently, we demonstrate successful modulation format conversions to 50-Gbps-class QPSK and 100-Gbps-class 16QAM signals. In addition, we discuss the format conversion performance when the input PAM4 signals are degraded owing to intra-DC transmission.

The remainder of this paper is organized as follows. In Sect. 2, we describe the operation principles of the proposed modulation format conversions. Section 3 describes the design of the SRN waveguide based on the waveguide mode analysis simulation. Section 4 presents the simulation results of the format conversion operation for 50-Gbps-class QPSK and 100-Gbps-class 16QAM signals. Finally, Sect. 5 presents the major conclusions of this paper.

2. Operation Principle

Figures 2(a) and (b) present overviews of the proposed PAM4 to QPSK and 16QAM converters using SRN waveguides, respectively. Both converters are based on XPM in the SRN waveguide for converting intensity modulation to phase modulation. For the PAM4 to QPSK conversion, a PAM4 signal at a λ_1 wavelength and a continuous wave (CW) light at λ_0 as a probe light are launched into an SRN waveguide. The phase of the probe light is modulated via XPM, which is driven by the PAM4 signal in the SRN waveguide. The phase change of the probe light due to XPM is expressed as

$$\phi^{(j)} = 2\gamma L_{\text{eff}} P^{(j)} \quad (j = 0, 1, 2, 3), \quad (1)$$

where γ and L_{eff} denote the nonlinear coefficient and effective length of the waveguide, respectively. The effective length is defined by

$$L_{\text{eff}} = \frac{1 - \exp(-\alpha L)}{\alpha}, \quad (2)$$

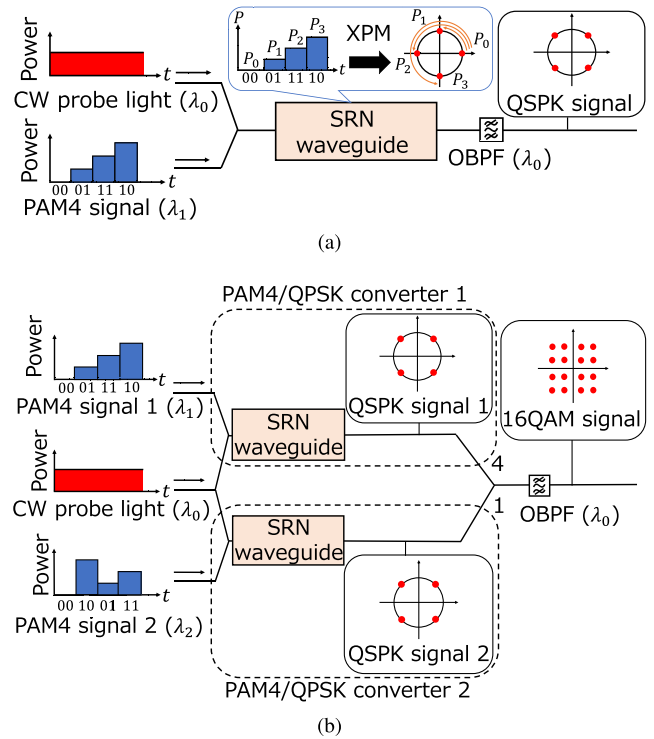


Fig. 2 Principles of (a) all-optical PAM4 to QPSK and (b) PAM4 to 16QAM conversions.

where α and L represent the attenuation constant and waveguide length, respectively. In addition, $P^{(j)}$ denotes the power level of the PAM4 signal, while the subscript j represents the information bit sequences of the PAM4 signal. The power level $P^{(j)}$ is adjusted such that $\phi^{(j)}$ are $0, \pi/2, \pi,$ and $3\pi/2$. By extracting the probe light component via an optical bandpass filter (OBPF), the converted QPSK signal at λ_0 can be obtained.

In the PAM4 to 16QAM converter, the $2 \times$ PAM4 signals are aggregated into a 16QAM signal. The PAM4/16QAM converter comprises two PAM4/QPSK converters and a 4:1 optical coupler (OC). PAM4 signals 1 and 2 at λ_1 and λ_2 are launched into the upper and lower SRN-waveguide-based PAM4/QPSK converters, respectively. Meanwhile, a CW probe light at λ_0 is launched into both SRN waveguides. At the upper SRN waveguide, PAM4 signal 1 is converted to QPSK signal 1 as described above. Similarly, QPSK signal 2 is generated from PAM4 signal 2 in the lower SRN waveguide. By coupling QPSK signals 1 and 2 at a power ratio of 4:1 and filtering the modulated probe light, a 16QAM signal is generated at the output of the converter.

3. Design of SRN Waveguide

3.1 Required Power for Modulation Format Conversion

As defined in Eqs. (1) and (2), the signal power required to obtain the desired phase rotation by XPM is determined by the nonlinear coefficient of the optical waveguide γ , waveguide length L , and loss α . Figure 3 presents the average sig-

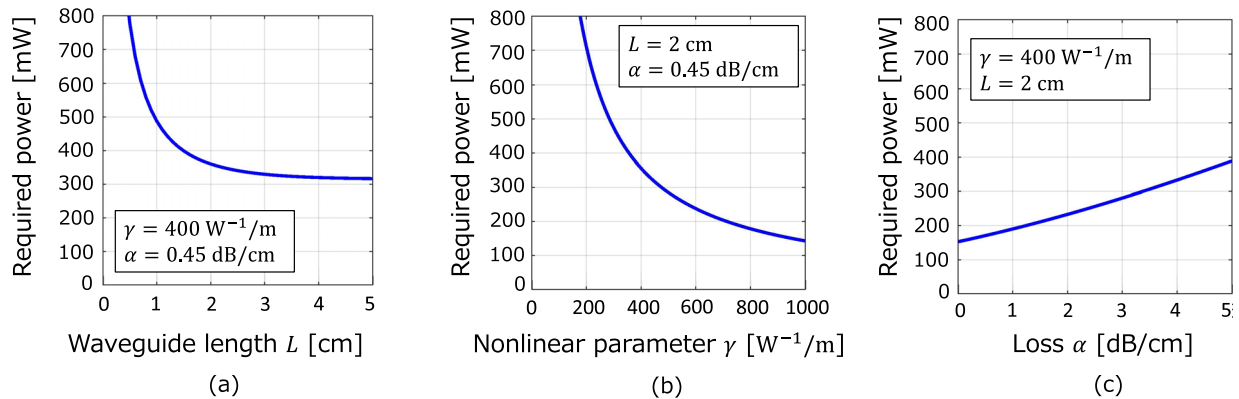


Fig. 3 Required Power for PAM4/QPSK conversion with varying (a) waveguide length, (b) nonlinear efficient, and (c) propagation loss.

nal power required for PAM4/QPSK conversion. Figure 3(a) shows the average signal power required for PAM4/QPSK conversion with γ of $400 \text{ W}^{-1}/\text{m}$ and varying L values. Figure 3(b) presents the results for a waveguide length of 2 cm and varying γ values. The loss α of the SRN waveguide was set to 4.5 dB/cm [17]. From the results in Figs. 3(a) and (b), the required signal power reduces when the nonlinear coefficient and waveguide length increase. The required signal power does not change significantly for a sufficiently long waveguide owing to the loss effect. For example, when the waveguide length is 2 cm or longer, the required signal power is 300–360 mW. Here, the waveguide length L is set to 2 cm. Figure 3(c) presents the results with γ of $400 \text{ W}^{-1}/\text{m}$, L of 2 cm, and varying α . Although the required signal power is 360 mW for a loss of 4.5 dB/cm, it can be reduced to less than 200 mW for a loss of 1 dB/cm. Here, the waveguide loss is set to 4.5 dB/cm as a representative value, which is reported in [17]. However, there is room for improvement in the propagation loss of the SRN waveguide by developing the deposition process. To keep the required signal power small, we must design a waveguide with a high nonlinear coefficient when the loss and length are limited. In this study, the waveguide length and loss were set to 2 cm and 4.5 dB/cm for the simulation, respectively.

3.2 Characteristics of SRN Waveguide

The optical waveguide adopted for format conversion in this study is an embedded square optical waveguide comprising a core of SRN and a cladding of SiO_2 . Several studies have been conducted on the fabrication of SRN based on chemical vapor deposition (CVD), such as inductively coupled plasma CVD (ICP-CVD), plasma-enhanced CVD (PECVD), and low-pressure CVD (LPCVD) [15]–[17]. The film composition and optical properties can be controlled by varying the process conditions, for example, gas ratio, temperature, and radio frequency (RF) power of the plasma source. However, the process must be designed to reduce the N-H bonds that induce propagation loss at telecommunication wavelengths. Further studies on reducing the loss are still required

Considering Kramers-Kronig and Miller's rule, the Kerr nonlinear refractive index n_2 increases as the refractive index increases, i.e., the ratio of Si:N increases. However, SRN with a considerably high refractive index has a too-low bandgap energy, which induces the TPA effect at telecommunication wavelengths. Fabrication was reported at the highest Si:N ratio of 7:3 with a bandgap of 2.1 eV, which achieves a high nonlinear refractive index and circumvents the TPA [17]. In this study, the composition ratio of SRN was assumed to be Si_7N_3 . In addition, the refractive index of SRN was calculated using the Sellmeier equation, assuming an amorphous compound with an amorphous Si to stoichiometric Si_3N_4 ratio of 19:21. The refractive index of SRN, $n_{\text{Si}_7\text{N}_3}(\omega)$, was obtained from

$$n_{\text{Si}_7\text{N}_3}(\omega) = 0.475n_{\text{Si}}(\omega) + 0.525n_{\text{Si}_3\text{N}_4}(\omega) \quad (3)$$

where n_{Si} and $n_{\text{Si}_3\text{N}_4}$ denote the refractive indices of Si and Si_3N_4 , respectively [21], [22].

We conducted the mode analysis of the SRN waveguide using the point-matching method [23], [24] to optimize a waveguide dimension for the modulation format conversion. The details of the point matching method are described in Appendix A. Owing to the large difference in refractive index between the core and cladding, the effective mode area A_{eff} and nonlinear parameter γ were calculated using the following equations [25]:

$$A_{\text{eff}} = \frac{Z_0^2}{n_{\text{core}}^2(\omega)} \frac{\left| \iint_{\text{total}} \text{Re} \{ E_x H_y - E_y H_x \} dx dy \right|^2}{\iint_{\text{core}} (E_x^2 + E_y^2)^2 dx dy} \quad (4)$$

$$\gamma = \frac{\omega_0 n_2}{c A_{\text{eff}}} \quad (5)$$

where Z_0 , $n_{\text{core}}(\omega)$, and c denote the characteristic impedance in a vacuum, the refractive index of the core, and the speed of light, respectively. The Kerr nonlinear refractive index of SRN is set to $2.8 \times 10^{-13} \text{ cm}^2/\text{W}$ [17].

Figure 4 presents the calculated results for the group velocity dispersion (GVD) parameter β_2 , third-order dispersion (TOD) parameter β_3 , and nonlinear coefficient γ of a

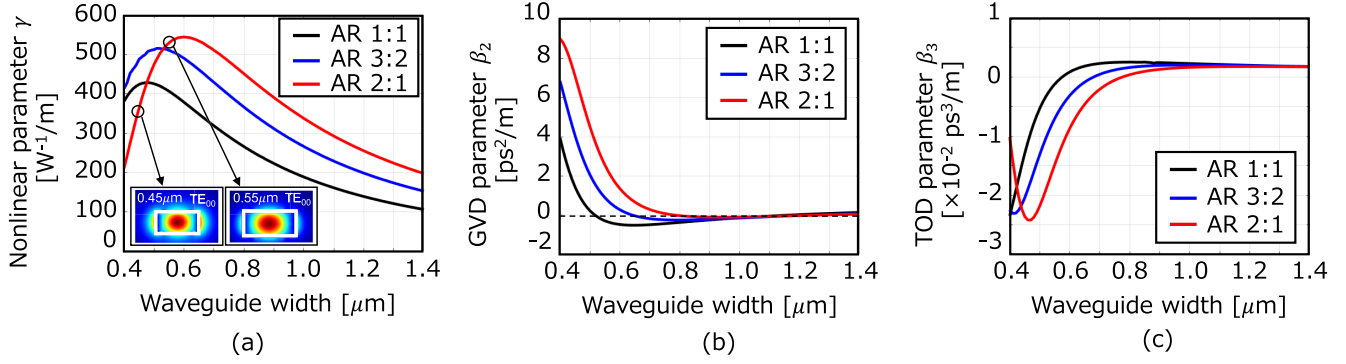


Fig. 4 Characteristics of the SRN waveguide: (a) Nonlinear parameter γ , (b) GVD parameter β_2 , and (c) TOD parameter β_3 .

Table 1 Waveguide parameters (AR 1:2).

Width (μm)	γ (W^{-1}/m)	β_2 (ps^2/m)	β_3 ($\times 10^{-2} \text{ps}^3/\text{m}$)
0.45	363	7.10	-2.42
0.50	475	4.50	-2.18
0.55	529	2.55	-1.48
0.60	544	1.35	-0.87

quasi-TE mode (TE_{00}) at a wavelength of 1550 nm. The results were calculated by varying the core width and aspect ratio (AR) of the SRN waveguide. In this study, the aspect ratio is defined as the ratio between the core width and height of the cross section of the waveguide (width:height). When AR was 2:1, the largest γ was achieved for the core width of 0.6 μm . β_2 decreased as the core width increased, and β_2 was close to zero for the core width above 0.7 μm . The representative values for an AR of 2:1 are presented in Table 1.

4. Numerical Simulation

4.1 Simulation Model

Numerical simulations were conducted to demonstrate the feasibility of the proposed modulation format conversions. Figure 5 illustrates the basic simulation model. PAM4 signals at 26.6 Gbaud were generated using a random bit sequence. The probe light wavelength λ_0 was set to 1550 nm. The wavelengths of the PAM4 signals were identical ($\lambda_1 = \lambda_2$) and varied from 1520 to 1580 nm. The power of the probe light was set to 0 dBm, and the power of the PAM4 signal was adjusted to satisfy Eq. (1). The PAM4 signals and probe light were input to the modulation format converters. The complex envelope amplitude $E(z, t)$ of the electric field in the SRN waveguide is described by the following nonlinear Schrödinger equation, which accounts for dispersion, nonlinearity, and losses [26],

$$i \frac{\partial E}{\partial z} - \frac{\beta_2}{2} \frac{\partial^2 E}{\partial t^2} - i \frac{\beta_3}{6} \frac{\partial^3 E}{\partial t^3} + \gamma |E|^2 E = -i \frac{\alpha}{2} E, \quad (6)$$

where z and t denote the propagation distance and time measured in a moving coordinate with the group velocity, respec-

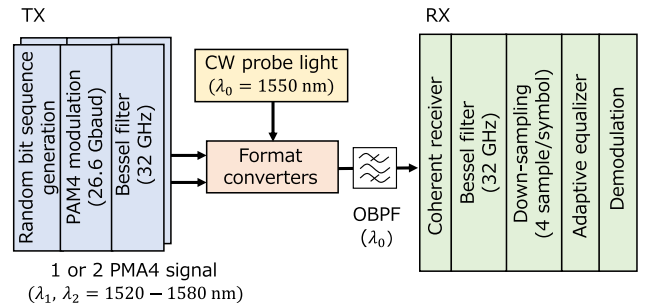


Fig. 5 Basic simulation model.

tively. In the simulations, the output optical field of the SRN waveguide was calculated numerically using the split-step Fourier method.

At an optical receiver, a high-order Bessel filter such as the fourth and fifth order Bessel filter is often used as an electrical low-pass filter for eliminating high-frequency components and shaping [27], [28]. We employed a fourth order Bessel filter in this simulation. An adaptive equalization was conducted with a decision-directed least mean square (DD-LMS) algorithm at the receiver. Before the adaptive equalization, downsampling to four sample/symbol was performed. For the demodulation of the converted signal, the number of tap coefficients of the LMS should be set to seven or more. In this simulation, we employed a sufficiently large number of tap coefficients at a total of 61 because it can compensate for the dispersion effects of the transmission of the PAM4 signal discussed in Sect. 4.2.3 and the converted signals in the inter-DC networks in our future work. Each adaptive equalizer was trained by the optimized step size that minimizes the evaluation function.

A coupling loss between the fiber and SRN waveguide is a significant issue. We evaluated the effect of the coupling loss on the format converter. Fig. 6(a) illustrates the modified simulation model from Fig. 5. When a large coupling loss exists, a higher input power of the PAM4 signal is required and the converted QPSK and 16QAM signal need to be amplified. The optical amplifiers were added before and after the SRN waveguide-based converter. The power spectral density N_o of the amplified spontaneous emission (ASE)

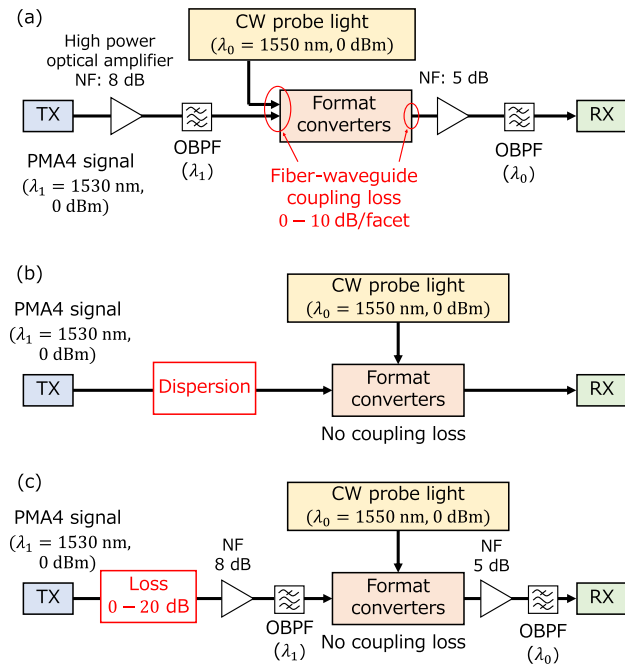


Fig. 6 Modified simulation model.

white noise at the output of the optical amplifier is described by [30]

$$N_o = h\nu n_{sp}(G - 1), \quad (7)$$

where n_{sp} is the spontaneous emission factor, G is the optical amplifier gain, h is Planck's constant, and ν is the optical frequency. When the gain is sufficiently large, the OSNR of the output signal depends on the input signal power and n_{sp} ($\sim NF/2$). The OSNR is significantly degraded after the second amplifier when the power of the converted QPSK signal is reduced by the coupling loss. Namely, the OSNR is degraded at the amplifier after the converter (amplification of the QPSK and 16QAM signals) rather than that before the converter (amplification of the PAM4 signal).

In addition, we investigated the performance of the PAM4/QPSK conversion when a large coupling loss exists and the input PAM4 signal is distorted owing to the transmission in an intra-DC network. Fig. 6(b) and (c) illustrate the modified simulation model from Fig. 5 to evaluate the effect of the PAM4 signal distortion. Before the modulation format conversion, we separately added the distortions to the PAM4 signal via the following two effects: (b) Dispersion and (c) noise. To investigate (b) dispersion effect, the PAM4 signal was dispersed by adding an accumulated dispersion from 0 to 150 ps/nm. For the investigation of (c) noise effect, we inserted a loss from 0 to 10 dB and optical amplifications before and after the converters. To investigate the effects of the coupling loss and PAM4 signal distortion, the wavelength of the signal light of the PAM4 signal and the core width of the waveguide were set to 1530 nm and 0.45 μm , respectively.

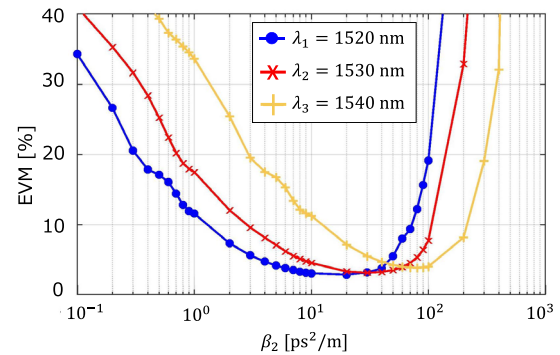


Fig. 7 EVM of the converted QPSK signal when varying β_2 .

4.2 Simulation Results

4.2.1 SRN Waveguide for Modulation Format Conversion

To consider the suitable SRN waveguide dimension for the proposed all-optical PAM4/QPSK and PAM4/16QAM conversions, we investigated the β_2 dependence on the conversion performance. We set γ to 400 W^{-1}/m and varied β_2 while observing the signal quality after conversion. The wavelength of the PAM4 signal λ_1 was set to three different values of 1520, 1530, and 1540 nm. Figure 7 illustrates the EVM of the QPSK signal after the all-optical PAM4/QPSK conversion. For all the wavelengths, the EVM increased when β_2 approached zero. This is because the probe light was amplified depending on the power level of the PAM4 signal owing to the effect of optical parametric amplification (OPA) when β_2 was approached zero. However, the EVM increased when β_2 increased above 10^2 owing to the walk-off effect. The group velocities of the probe and PAM4-signal lights differ according to the GVD. When the relative time at the input/output of the SRN waveguide between the probe light and PAM4 signal deviates significantly, an inter-symbol interference occurs and the converted signal is distorted.

To avoid the signal deterioration in the conversion process owing to OPA and the walk-off effects, β_2 values should be several ps^2/m to several tens of ps^2/m . In addition, a large value of γ is desirable for high conversion efficiency. Considering the waveguide characteristics illustrated in Fig. 4, the SRN waveguide with an AR of 2:1 and a core width of 0.45–0.60 μm is adopted for the proposed modulation format converters in this study. A larger β_2 can be achieved even for AR of 3:2 and 1:1 by reducing the waveguide width. For example, β_2 of 7.0 ps^2/m and γ of 348 W^{-1}/m can be obtained when the waveguide width is 0.387 μm for AR of 3:2. However, the waveguide characteristics become more sensitive to the manufacturing error (the shift from the target width) as the width reduces. This is the reason why we selected the AR of 2:1 in this study.

4.2.2 Performance of the Modulation Format Conversion

We evaluated the basic performance of the proposed for-

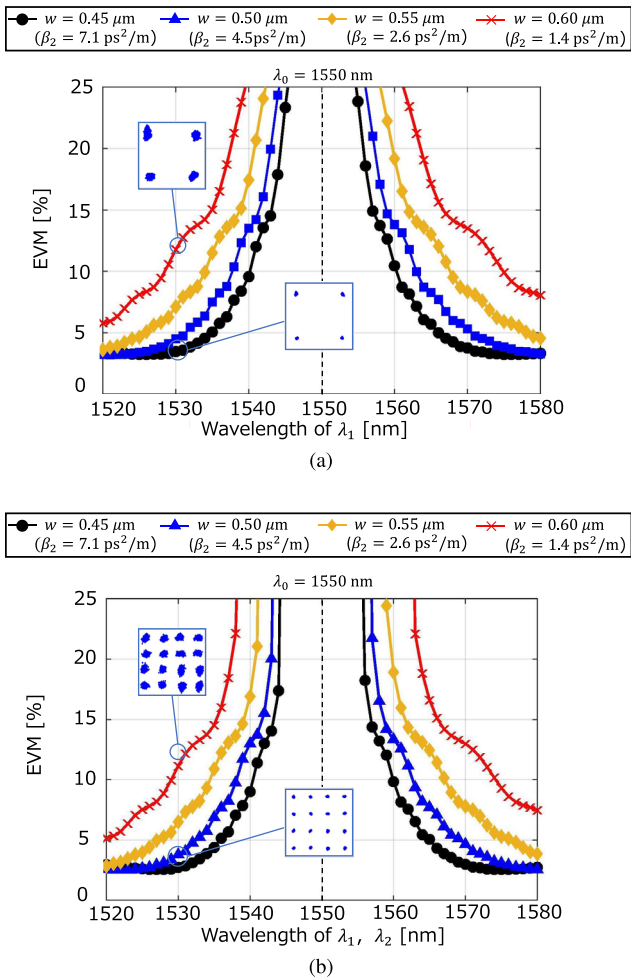


Fig. 8 EVM and representative constellation diagrams of converted (a) QPSK and (b) 16QAM signals.

mat conversion. In this section, we assume that the input PAM4 signal is not distorted, the fiber-waveguide coupling loss is negligible, and the propagation loss is a fixed value of 4.5 dB/cm. Figure 8 presents the EVM of the converted QPSK and 16QAM signals with different wavelengths (λ_1 and λ_2) of the PAM4 signals and waveguide width w . Representative constellation diagrams of the converted QPSK and 16QAM signals are also presented in Fig. 8. The EVM increased when the wavelength of the PAM4 signal light was close to the probe light wavelength of 1550 nm. This is because the probe light was amplified depending on the power level of the PAM4 signal, namely the bit sequence, owing to the OPA effect, which induced the change in the power of the converted signal depending on the bit sequence. When the core width of the waveguide was $0.60 \mu\text{m}$ ($\beta_2 = 1.2 \text{ ps}^2/\text{m}$), the EVM was larger than when the core width was $0.45 \mu\text{m}$ ($\beta_2 = 6.7 \text{ ps}^2/\text{m}$) owing to the OPA. When the core width was $0.45 \mu\text{m}$ and the wavelength difference between the PAM4 signal and the probe light was 10 nm or more, the EVM of the converted QPSK and 16QAM signals were both below 10%.

Figure 9 presents the BER curves of the converted

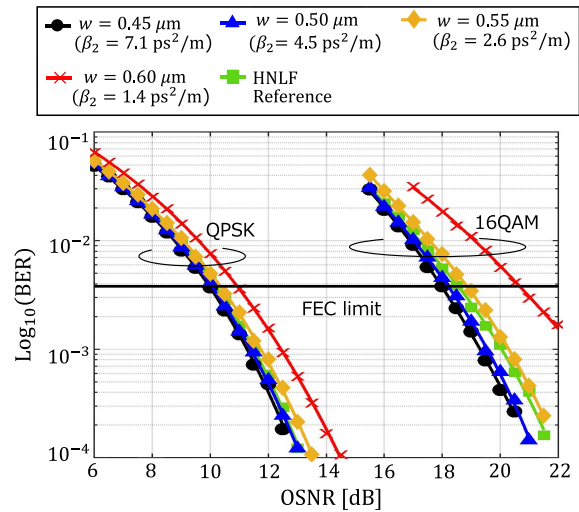


Fig. 9 BER curve.

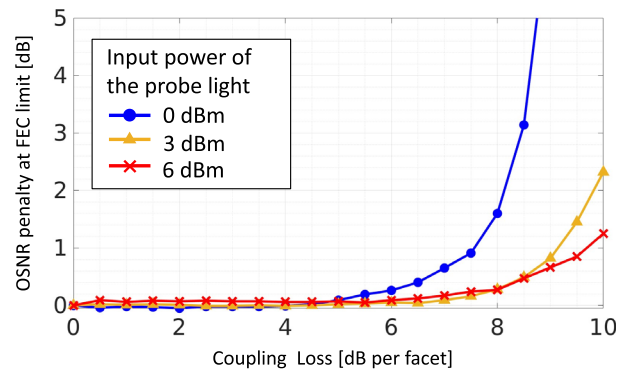


Fig. 10 OSNR penalty at the FEC limit with varying coupling loss.

QPSK and 16QAM signals when the wavelength of the PAM4 signal light was 1530 nm. The BER curve of the converter using HNLF is also presented in Fig. 9 for comparison [29]. The optical signal-to-noise ratio (OSNR) penalty was observed by OPA when the core width of the channel was $0.60 \mu\text{m}$. However, when the core width of the waveguide was $0.45 \mu\text{m}$ or $0.50 \mu\text{m}$, the BER characteristics for both the QPSK and 16QAM signals were comparable to that for the HNLF-based conversions.

4.2.3 Effect of the Loss in the Converter

Figure 10 shows the OSNR penalty of the converted QPSK signal at the FEC limit when varying the coupling loss. The OSNR penalty increased as the coupling loss increased. However, the penalty can be compensated by increasing the input power of the probe light, namely, by increasing the input power of the converted signal into the optical amplifier. The fiber-SRN waveguide coupling loss is approximately 7.0 dB per facet [17]. The OSNR penalty due to the coupling loss of 7.0 dB can be maintained below 0.3 dB when the input power of the probe light is 3 or 6 dBm.

The insertion loss including the coupling loss and prop-

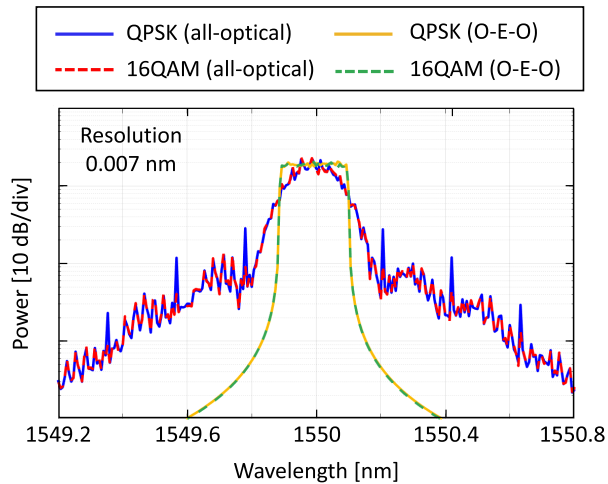


Fig. 11 Spectra of the 16QAM signals generated by the all-optically and OEO converters.

agation loss in the SRN increases when the core size and width w decreases. However, the OSNR penalty due to the propagation loss can be compensated by increasing the probe light power as well as in the case of the coupling loss.

4.2.4 Comparison with OEO Conversion

In the conventional system, QPSK and 16QAM signals are generated by an optical-to-electrical-to-optical (OEO) conversion and an IQ modulator at gateway nodes. The all-optically converted QPSK and 16QAM signals contain a frequency chirp caused by the XPM in the SRN waveguide. Figure 11 shows the spectra of the QPSK and 16QAM signals generated by the all-optically and OEO converters. In the case of the OEO converter, the 16QAM signal was Nyquist-shaped by a root-raised cosine filter with a roll-off factor of 0.01 assuming the use of the IQ modulator and digital signal processing. It was confirmed that the frequency spectrum of the all-optically converted signals was broadened because of the frequency chirp caused by the XPM in the SRN. The transmission characteristics of the all-optically converted QPSK and 16QAM signals using the XPM in an HNLF were reported in [31]. The spectral broadening of the 16QAM signal generated by the SRN-based converter is similar to that generated by the HNLF-based converter in [31]. It is inferred from the spectral characteristics that the all-optically converted signal using the SRN is more affected by the ASE noise, however, more resistant to the nonlinear distortion in a long-haul fiber transmission compared with the OEO converted signal, as well the case of the HNLF-based converter. The detailed analysis of the transmission characteristics of the converted signal need to be studied further.

4.2.5 Effect of the Input PAM4 Signal

Figure 12 presents the EVM of the converted QPSK signal when the PAM4 signal is distorted by the dispersion effect.

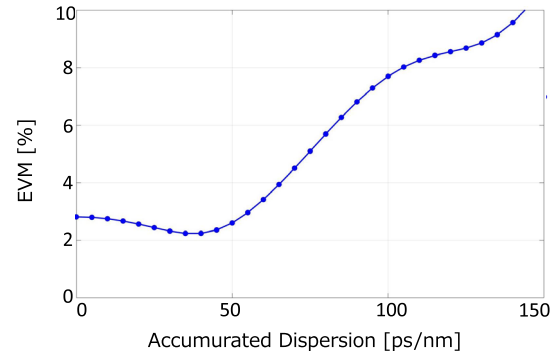


Fig. 12 EVM of the converted QPSK signal when adding dispersion effect to the PAM4 signal.

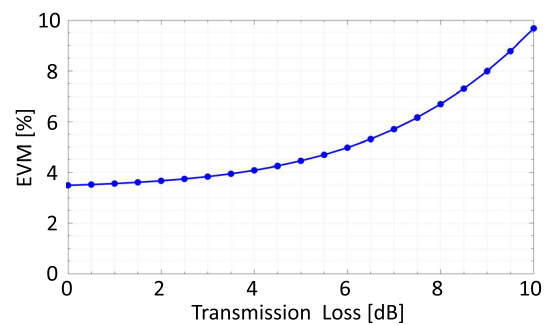


Fig. 13 EVM of the converted QPSK signal when adding noise effect to the PAM4 signal.

When the accumulated dispersion was less than 140 ps/nm, the EVM was less than 10%. In IEEE802.3bs [32], 8 WDM channels of wavelengths from 1273.55 to 1309.14 nm in the O-band were adopted. Assuming an SSMF with a zero dispersion wavelength of 1300 nm and dispersion slope of $0.092 \text{ ps/nm}^2/\text{km}$ [33], the range of dispersion parameter is from -2.4 to 0.8 ps/nm/km (1273.55–1309.14 nm). In this case, 2-km and 10-km transmissions of 400Gbase-FR-8 and 400Gbase-ER-8 are acceptable because the range of the accumulated dispersion is from -24 to 8 ps/nm with the 10-km transmission. Note that the wavelength converter from the O- to C-band is necessary when the PAM4 signal is transmitted using the O-band in the intra-DC network.

Figure 13 presents the EVM of the converted QPSK signal when the PAM4 signal is distorted by the noise effect (loss and optical amplification). When the loss was less than 10 dB, the EVM was less than 10%. Assuming the maximum loss of 0.4 dB/km in the O-band [33], a loss of a 25 km transmission is acceptable to maintain the EVM below 10%.

Finally, we discuss the synchronization between the two PAM4 signals. The PAM4 to 16QAM conversion, which includes an aggregation of two PAM4 signals, requires an adjustment of the input timing between the two PAM4 signals. However, this decreases the flexibility of the optical signal processing. To address this issue, the application of a multi-stage adaptive equalizer to demodulation for a 16QAM signal optically aggregated from the PAM4 signals

using an HNLF-based format converter was proposed [34]. Using the multi-stage equalizer, the 16QAM signal can be demodulated regardless of the time difference between the two PAM4 signals input to the converter. We expect that the multi-stage equalizer can be applied to the 16QAM signal generated by the SRN-based converter as well.

5. Conclusions

We proposed novel all-optical PAM4 to QPSK and 16QAM conversions using SRN waveguide. First, we designed the modulation format converters via a mode analysis of the SRN waveguide and demonstrated that suitable parameters of the format converters, such as the GVD parameter β_2 of several ps^2/m and high nonlinear parameter γ , were obtained when the core widths were $0.45\text{--}0.55\ \mu\text{m}$. Consequently, using the designed SRN waveguide, we numerically demonstrated the successful conversions from 50-Gbps-class PAM4 signals to 50-Gbps-class QPSK and 100-Gbps-class 16QAM signals. Using an appropriate waveguide width and wavelength, the BER characteristics of the converted signals were comparable to those achieved via HNLF-based conversions. Subsequently, we demonstrated the effects of the waveform distortion of the PAM4 signal due to chromatic dispersion and noise.

Acknowledgments

A part of the results in this study was obtained from the commissioned research by Beyond 5G R&D Promotion under Project 01401, National Institute of Information and Communications Technology (NICT), Japan. This study was partially supported by The GMO Internet Foundation, Japan. The authors would like to thank Mr. Yuki Ishihara for his cooperation in the analysis of the waveguide and the helpful discussions.

References

- [1] E. Yamazaki, S. Yamanaka, Y. Kisaka, T. Nakagawa, K. Murata, E. Yoshida, T. Sakano, M. Tomizawa, Y. Miyamoto, S. Matsuoka, J. Matsui, A. Shibayama, J. Abe, Y. Nakamura, H. Noguchi, K. Fukuchi, H. Onaka, K. Fukumitsu, K. Komaki, O. Takeuchi, Y. Sakamoto, H. Nakashima, T. Mizuochoi, K. Kubo, Y. Miyata, H. Nishimoto, S. Hirano, and K. Onohara, "Fast optical channel recovery in field demonstration of 100-Gbit/s Ethernet over OTN using real-time DSP," *OSA Opt. Express*, vol.19, no.14, pp.13179–13184, June 2007.
- [2] H. Maeda, T. Kotanigawa, K. Saito, M. Yokota, S. Yamamoto, M. Suzuki, and T. Seki, "Field trial of simultaneous 100-Gbps and 400-Gbps transmission using advanced digital coherent technologies," *Proc. Opt. Fiber Commun. Conf. (OFC2016)*, Anaheim, US, Paper W1K.4, March 2016.
- [3] J. Elbers, N. Eiselt, A. Dochhan, D. Rafique, and H. Griesser, "PAM4 vs coherent for DCI applications," *Proc. Signal Processing in Photonic Commun. (SPPCom)*, New Orleans, LA, USA, Paper SpTh2D.1, July 2017.
- [4] A.E. Willner, A. Fallahpour, F. Alishahi, Y. Cao, A.M.-Ariaei, A. Almainan, P. Liao, K. Zou, A.N. Willner, and M. Tur, "All-optical signal processing techniques for flexible networks," *IEEE/OSA J. Lightw. Technol.*, vol.37, no.1, pp.21–35, Jan. 2019.
- [5] K. Mishina, D. Hisano, and A. Maruta, "All-optical modulation format conversion and applications in future photonic networks," *IEICE Trans. Electron.*, vol.E102-C, no.4, pp.304–315, April 2019.
- [6] K. Mishina, A. Maruta, S. Mitani, T. Miyahara, K. Ishida, K. Shimizu, T. Hatta, K. Motoshima, and K. Kitayama, "NRZ-OOK to RZ-BPSK modulation-format conversion using SOA-MZI wavelength converter," *IEEE/OSA J. Lightw. Technol.*, vol.24, no.10, pp.3751–3758, Oct. 2006.
- [7] K. Mishina, S. Kitagawa, and A. Maruta, "All-optical modulation format conversion from on-off keying to multiple-level phase-shift-keying based on nonlinearity in optical fiber," *OSA Opt. Express*, vol.15, no.13, pp.8444–8453, June 2007.
- [8] G. Huang, Y. Miyoshi, A. Maruta, and K. Kitayama, "All-optical technique for modulation format conversion from NRZ-OOK to RZ-16QAM employing nonlinear optical loop mirror with 1:2 coupler," *OSA Opt. Express*, vol.20, no.24, pp.27311–27321, Nov. 2012.
- [9] A. Fallahpour, A. Mohajerin-Ariaei, A. Almainan, Y. Cao, F. Alishahi, C. Bao, P. Liao, M. Ziyadi, B. Shamee, D. Starodubov, M. Tur, C. Langrock, M.M. Fejer, J. Touch, and A.E. Willner, "Demonstration of 30 Gbit/s QPSK-to-PAM4 data-format and wavelength conversion to enable all-optical gateway from long-haul to data center," *Proc. Opt. Fiber Commun. Conf. (OFC2018)*, San Diego, US, Paper W2A.22, March 2018.
- [10] A. Fallahpour, M. Ziyadi, A. Mohajerin-Ariaei, Y. Cao, A. Almainan, F. Alishahi, C. Bao, P. Liao, B. Shamee, L. Paraschis, M. Tur, C. Langrock, M.M. Fejer, J. Touch, and A.E. Willner, "Experimental demonstration of tunable optical de-aggregation of each of multiple wavelength 16-QAM channels into two 4-PAM channels," *Proc. Opt. Fiber Commun. Conf. (OFC2017)*, Los Angeles, US, Paper Th4I.6, March 2017.
- [11] T. Kodama, T. Miyazaki, and M. Hanawa, "Seamless PAM-4 to QPSK modulation format conversion at gateway for short-reach and long-haul integrated networks," *Proc. 44th European Conf. on Opt. Commun. (ECOC2018)*, Roma, Italy, Paper We3H, Sept. 2018.
- [12] Y. Matsumoto, K. Mishina, D. Hisano, and A. Maruta, "All-optical PAM4 to 16QAM modulation format conversion using nonlinear optical loop mirror and 1:2 coupler," *IEICE Trans. Commun.*, vol.E103-B, no.11, pp.1272–1281, Nov. 2020.
- [13] C. Langrock, S. Kumar, J.E. McGeehan, A.E. Willner, and M.M. Fejer, "All-optical signal processing using χ^2 nonlinearities in guided-wave devices," *IEEE/OSA J. Lightw. Technol.*, vol.24, no.7, pp.2579–2592, July 2006.
- [14] J. Leuthold, C. Koos, and W. Freude, "Nonlinear silicon photonics," *Nature Photon.*, vol.4, pp.535–544, Aug. 2010.
- [15] D.T.H. Tan, K.J.A. Ooi, and D.K.T. Ng, "Nonlinear optics on silicon-rich nitride — A high nonlinear figure of merit CMOS platform," *OSA Photon. Res.*, vol.6, no.5, pp.B50–B66, May 2018.
- [16] C. Lacava, S. Stankovic, A.Z. Khokhar, T.D. Bucio, F. Gardes, G.T. Reed, D.J. Richardson, and P. Petropoulos, "Si-rich silicon nitride for nonlinear signal processing applications," *Sci. Rep.*, vol.7, no.22, pp.1–13, Feb. 2017.
- [17] K.J.A. Ooi, D.K.T. Ng, T. Wang, A.K.L. Chee, S. Ng, Q. Wang, L. Ang, A. Agarwal, L. Kimerling, and D.T.H. Tan, "Pushing the limits of CMOS optical parametric amplifiers with USRN:Si7N3 above the two-photon absorption edge," *Nat. Commun.*, vol.8, no.13878, pp.1–10, Jan. 2017.
- [18] M.R. Dizaji, C.J. Krücker, A. Fülöp, P.A. Andrekson, V. Torres-Company, and L.R. Chen, "Silicon-rich nitride waveguides for ultra-broadband nonlinear signal processing," *OSA Opt. Express*, vol.25, no.11, pp.12100–12 08, May 2017.
- [19] Y. Ishihara, M. Roy, C.A.R. Pineda, A. Maruta, and K. Mishina, "Wideband simultaneous wavelength conversion of multiple WDM channels using silicon-rich nitride waveguide," *IEEE Photon. J.*, vol.14, no.6, pp.1–7, Dec. 2022.
- [20] Y. Fujihara, K. Mishina, A. Sueyoshi, A.R. de Paula, and A. Maruta, "All-optical PAM4 to QPSK and 16QAM conversions using Si-rich

SiN waveguides,” Proc. 27th Optoelectronics and Commun. Conf./ Int. Conf. on Photon. in Switching and Computing 2022 (OECC/PSC 2022), Toyama, Japan, Paper WP-F-2, July 2022.

- [21] B. Tatian, “Fitting refractive-index data with the Sellmeier dispersion formula,” OSA Appl. Opt., vol.23, no.24, pp.4477–4485, Dec. 1984.
- [22] K. Luke, Y. Okawachi, M.R.E. Lamont, A.L. Gaeta, and M. Lipson, “Broadband mid-infrared frequency comb generation in a Si₃N₄ microresonator,” OSA Opt. Lett., vol.40, no.21, pp.4823–4826, Nov. 2015.
- [23] J.E. Goell, “A circular-harmonic computer analysis of rectangular dielectric waveguides,” Bell Syst. Tech. J., vol.48, no.7, pp.2133–2160, Sept. 1969.
- [24] E. Yamashita, Analysis Methods for Electromagnetic Wave Problems, Artech House, London, UK, 1990.
- [25] C. Koos, L. Jacome, C. Poulton, J. Leuthold, and W. Freude, “Nonlinear silicon-on-insulator waveguides for all-optical signal processing,” OSA Opt. Express, vol.15, no.10, pp.5976–5990, May 2007.
- [26] G.P. Agrawal, Nonlinear Fiber Optics, 5th ed., Academic Press, Cambridge, MA, 2012.
- [27] J.M.D.D. Mendinueta, P. Bayvel, and B.C. Thomsen, “Digital light-wave receivers: An experimentally validated system model,” IEEE Photon. Technol. Lett., vol.23, no.6, pp.338–340, March 2011.
- [28] S.J. Savory, “Digital filters for coherent optical receivers,” OSA Opt. Express, vol.16, no.2, pp.804–817, Jan. 2008.
- [29] A. Sueyoshi, Y. Matsumoto, K. Mishina, D. Hisano, and A. Maruta, “Spectral efficiencies and transmission characteristics of all-optical PAM4 to QPSK and 16QAM converted signals,” Proc. 25th Optoelectronics and Communications Conference (OECC 2020), Taipei, Taiwan, Paper T2-1.4, Oct. 2020.
- [30] S. Bottacchi, Noise and Signal Interference in Optical Fiber Transmission Systems, Wiley, Chichester, UK, 2008.
- [31] A. Sueyoshi, D. Hisano, A. Maruta, and K. Mishina, “Transmission characteristics of all-optically converted QPSK and 16QAM signals,” Opt. Commun., vol.537, p.129432, June 2023.
- [32] IEEE P802.3bs/D3.4, Draft standard for ethernet amendment: media access control parameters, physical layers and management parameters for 200 Gb/s and 400 Gb/s, Oct. 2017.
- [33] ITU-T, G.652, “Characteristics of a single-mode optical fibre and cable,” Nov. 2016.
- [34] A. Sueyoshi, K. Mishina, D. Hisano, and A. Maruta, “Multi-stage adaptive equalization for all-optical-aggregated 16QAM signal,” IEICE Commun. Express, vol.11, no.5, pp.183–188, May 2022.

Appendix: Point-Matching Method

The general solution of the electromagnetic field in a rectangular waveguide is given by circular cylindrical harmonic functions, namely, the Bessel’s functions $J_n(\cdot)$ or the modified Bessel’s functions $K_n(\cdot)$ multiplied by sinusoidal functions. The longitudinal components of electromagnetic fields E_z and H_z can be expressed as

$$E_{z,1} = \sum_{n=0}^{\infty} a_n J_n(hr) \sin(n\theta + \phi_n) \exp\{i(\beta z - \omega t)\}, \quad (\text{A}\cdot 1)$$

$$H_{z,1} = \sum_{n=0}^{\infty} b_n J_n(hr) \cos(n\theta + \psi_n) \exp\{i(\beta z - \omega t)\}, \quad (\text{A}\cdot 2)$$

$$E_{z,2} = \sum_{n=0}^{\infty} c_n K_n(pr) \sin(n\theta + \phi_n) \exp\{i(\beta z - \omega t)\}, \quad (\text{A}\cdot 3)$$

$$H_{z,2} = \sum_{n=0}^{\infty} d_n K_n(pr) \cos(n\theta + \psi_n) \exp\{i(\beta z - \omega t)\}, \quad (\text{A}\cdot 4)$$

where a_n , b_n , c_n , and d_n represent the expansion coefficients determined by the boundary conditions. h and p denote propagation constants in the cross-sectional direction, ϕ_n and ψ_n are arbitrary phase angles, and β represents the propagation constant in the z -axis direction. In addition, subscripts 1 and 2 represent the core and cladding regions, respectively. Subsequently, the electromagnetic field problem is approximately addressed by considering a finite number of matching points on the core and cladding boundaries and then satisfying the boundary conditions at these points.

Yuto Fujihara received his B.E. degree in Electrical, Electronic and Information Engineering from Osaka University, Osaka, Japan, in 2022. He is currently working toward his M.E. degree at Osaka University. Mr. Fujihara is a Student Member of the Institute of Electronics, Information, and Communication Engineers of Japan.



Asahi Sueyoshi received his B.E. and M.E., in Electrical, Electronic, and Information Engineering from Osaka University, Osaka, Japan, in 2020 and 2022, respectively.



Alisson Rodrigues de Paula received his B.E. degree in Electrical Engineering from Universidade Federal de Goiás, Brazil, in 2018. He received his M.E. degree in Photonic Integrated Circuits, Sensors and Network from Aston University, United Kingdom, and Scuola Superiore Sant’Anna, Italy, in 2021. Currently, he is working in CNRS CORIA laboratory, in France, with high-speed optic metrology applied to pulsed laser sources and imaging of ultra-short phenomena.



Akihiro Maruta received his B.E., M.E., and Ph.D. degrees in Communication Engineering from Osaka University, Osaka, Japan, in 1988, 1990, and 1993, respectively. In 1993, he joined the Department of Communications Engineering, Osaka University. Since 2016, he has been a Professor with the Department of Information and Communication Technology, Osaka University. His current research interests include optical fiber communication systems and all-optical signal processing. He is a Member of

the IEEE Photonics Society and Optica, and a Senior Member of IEICE, Japan.



Ken Mishina received his B.E., M.E., and Ph.D. degrees in Electrical, Electronic, and Information Engineering from Osaka University, Osaka, Japan, in 2005, 2007, and 2012, respectively. In 2007, he joined Shimadzu Corporation in Kyoto, Japan. Since 2018, he has served as Associate Professor in the Department of Information and Communication Technology at the Division of Electrical, Electronic, and Information Engineering, Graduate School of Engineering, Osaka University. His research

interests include optical fiber communication systems, all-optical signal processing, and photovoltaics. He is a Member of IEEE Photonics Society and IEICE, Japan.